

NLO supersymmetric QCD corrections to the $t\bar{b}H^-$ associated production at hadron colliders

Wu Peng², Ma Wen-Gan^{1,2}, Zhang Ren-You², Jiang Yi², Han Liang², and Guo Lei²

¹CCAST (World Laboratory), P.O.Box 8730, Beijing, 100080, People's Republic of China

²Department of Modern Physics, University of Science and Technology of China (USTC),
Hefei, Anhui 230026, People's Republic of China

Abstract

We present the next-to-leading order QCD corrected total cross sections and the distributions of the transverse momenta of the final anti-bottom-quark, top-quark and charged Higgs-boson for the processes of $p\bar{p}/pp \rightarrow t\bar{b}H^- + X$ in the minimal supersymmetric standard model(MSSM) at the Tevatron and the LHC. We find that the NLO QCD corrections significantly modify the leading-order distributions of the transverse momenta of final particles(p_T^b , p_T^t and $p_T^{H^-}$), and the total NLO QCD corrections reduce the dependence of the cross section on the renormalization and factorization scales, especially the NLO QCD corrected cross sections at the LHC are nearly independent of these scales. Our results show that the relative correction is obviously related to m_{H^-} and $\tan\beta$, and the total NLO QCD relative corrections can be beyond -50% at the Tevatron and approach -40% at the LHC in our chosen parameter space.

PACS: 12.60.Jv, 14.80.Cp, 14.65.Fy

1 Introduction

One of the major objectives of future high-energy experiments is to search for scalar Higgs bosons and investigate the symmetry breaking mechanism of the electroweak interactions. In the standard model (SM) [1], one doublet of complex scalar fields is introduced to spontaneously break the symmetry, leading to a single neutral Higgs boson H^0 . But there exists the problem of the quadratically divergent contributions to the corrections to the Higgs boson mass. That is the so-called naturalness problem. The supersymmetric (SUSY) extensions of the SM provide a possibility to solve this problem. In supersymmetric models, the quadratic divergences of the Higgs boson mass can be cancelled by loop diagrams involving the supersymmetric partners of the SM particles exactly. The most attractive and simplest supersymmetric extension of the SM is the minimal supersymmetric standard model (MSSM)[2, 3]. In this model, there are two Higgs doublets H_1 and H_2 to give masses to up- and down-type fermions. The Higgs sector consists of three neutral Higgs bosons, one CP -odd particle (A^0), two CP -even particles (h^0 and H^0), and a pair of charged Higgs bosons (H^\pm).

However, these Higgs bosons haven't been directly explored experimentally until now. If the charged Higgs boson is lighter than the top quark, it would probably be found at the upgraded Tevatron or at the future LHC through the $t \rightarrow bH^+$ decay channel[4]. Otherwise, if the charged Higgs boson is heavier than the top quark, there are three major channels to search the charged Higgs boson: (1)Charged Higgs boson pair production[5, 6, 7, 8, 9]; (2)Associated production of a charged Higgs boson with a W boson[10, 11]; (3)Associated production of a charged Higgs boson with a top quark[12]. The decay of the charged Higgs boson has two major channels: $H^- \rightarrow t\bar{b}$ [13], and $H^- \rightarrow \tau\bar{\nu}$ [14]

The associated production of a charged Higgs boson with a top quark ($pp/p\bar{p} \rightarrow tH^- + X$) seems to be the most promising channel[15]. Corresponding to ignoring or observing the final state anti-bottom quark experimentally, the cross section can be inclusive(ignore final state anti-bottom quark) or exclusive(observe final state anti-bottom quark). The inclusive and exclusive leading order subprocesses can be written as:

$$g\bar{b} \rightarrow tH^-, \quad (1.1)$$

$$gg \rightarrow t\bar{b}H^-, \quad qq \rightarrow t\bar{b}H^-, \quad (1.2)$$

respectively. The next-to-leading order(NLO) total cross section of the inclusive process has been studied in the SM QCD[16] and supersymmetric QCD[17].

In this paper, we calculate the total cross section of exclusive processes for the associated production of the charged Higgs boson with top quark and anti-bottom quark($pp/p\bar{p} \rightarrow t\bar{b}H^- + X$) in the MSSM at hadron colliders including the NLO QCD corrections. In section 2, we present the calculations of the leading order cross sections to $pp/p\bar{p} \rightarrow t\bar{b}H^- + X$ in the MSSM. In section 3, we present the calculations of the NLO QCD corrections to $pp/p\bar{p} \rightarrow t\bar{b}H^- + X$ in the MSSM. The numerical results and discussions are presented in section 4. Finally, a short summary is given.

2 The Leading Order Cross Sections

The exclusive $t\bar{b}H^-$ production mechanism at the parton level contributing to the hadronic processes $pp/p\bar{p} \rightarrow t\bar{b}H^- + X$, involves $q\bar{q}$ ($q = u, d$) annihilation and gluon-gluon fusion channels. The subprocess via the $q\bar{q}$ annihilation is written as

$$q(p_1)\bar{q}(p_2) \rightarrow t(p_3)\bar{b}(p_4)H^-(p_5), \quad (2.1)$$

And the subprocess via gluon-gluon fusion is denoted as

$$g(p_1)g(p_2) \rightarrow t(p_3)\bar{b}(p_4)H^-(p_5), \quad (2.2)$$

In above notations of these two channels, we use p_1, p_2 and p_3, p_4, p_5 to represent the four-momenta of the incoming partons and the outgoing particles respectively, and write them in brackets. The Feynman diagrams at leading order(LO) for the two subprocesses (2.1) and (2.2) are plotted in Fig.1 and Fig.2, separately. In Fig.1 both figures are gluon exchanging s-channel diagrams with a charged Higgs boson being radiated from anti-top-quark and bottom-quark, respectively. Fig.2(a-b), Fig.2(c-e) and Fig.2(f-h) belong to the s-channel, t-channel and u-channel diagram groups, respectively.

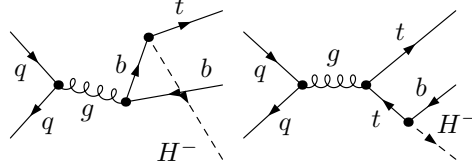


Fig. 1. The tree-level Feynman diagrams for $q\bar{q} \rightarrow t\bar{b}H^-$ subprocess.

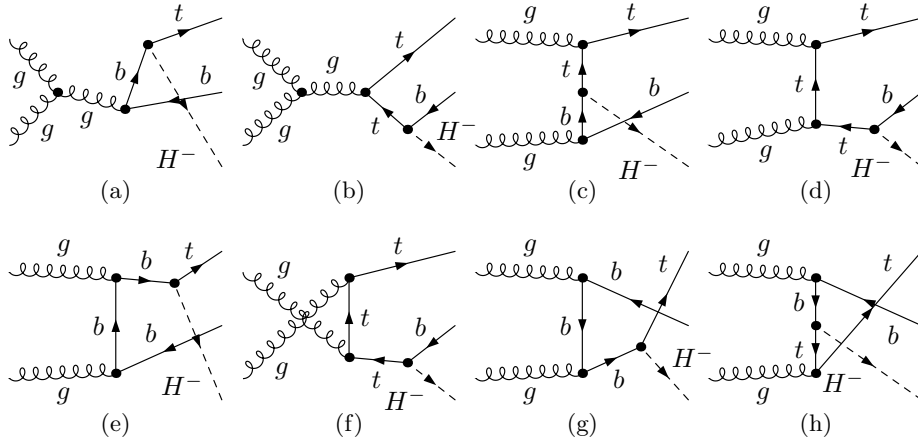


Fig. 2. The tree-level Feynman diagrams for $gg \rightarrow t\bar{t}h$ subprocess.

For the (2.1) subprocess $q\bar{q} \rightarrow t\bar{b}H^-$, the corresponding LO and NLO amplitudes can be expressed in the form as[19]:

$$M_{LO,NLO}^{q\bar{q}} = C^{q\bar{q}} A_{LO,NLO}^{q\bar{q}} \quad (2.3)$$

where $C^{q\bar{q}}$ is the only color factor involved in the LO amplitude of the subprocess $q\bar{q} \rightarrow t\bar{b}H^-$, which can be written as:

$$C^{q\bar{q}} = \lambda^c \otimes \lambda^c, \quad (2.4)$$

The first 3×3 $SU(3)$ Gell-Mann matrix λ^c arises from $q\bar{q}$ color state, the second Gell-Mann matrix λ^c arises from $t\bar{b}$ color state.

Similarly, the LO amplitude of the (2.2) subprocess $g\bar{g} \rightarrow t\bar{b}H^-$ can be expressed as:

$$M_{LO}^{gg} = \left(\frac{2}{3}C_1^{gg} + C_2^{gg} + C_3^{gg} \right) M_1^{gg} + \left(\frac{2}{3}C_1^{gg} - C_2^{gg} + C_3^{gg} \right) M_2^{gg}, \quad (2.5)$$

with

$$C_1^{gg} = \delta^{c_1 c_2} \mathbf{1}, \quad C_2^{gg} = i f^{c_1 c_2 c} \lambda^c, \quad C_3^{gg} = d^{c_1 c_2 c} \lambda^c, \quad (2.6)$$

$$M_1^{gg} = M_t^{gg} + \frac{1}{2} M_s^{gg}, \quad (2.7)$$

$$M_2^{gg} = M_u^{gg} - \frac{1}{2} M_s^{gg}, \quad (2.8)$$

where c_n ($n = 1, 2$) are the color indexes of incoming gluons, f^{abc} and d^{abc} are the $SU(3)$ antisymmetric and symmetric structure constants respectively, matrixes $\mathbf{1}$ and λ^c arise from $t\bar{b}$ color state. M_s^{gg} , M_t^{gg} and M_u^{gg} are the amplitude parts corresponding to the s-, t- and u-channel amplitude groups, respectively. Taking the trace of color factors, we get:

$$Tr(C_i^{gg\dagger} C_j^{gg}) = c_i^{gg} \delta_{jk} \quad \text{with} \quad c_1^{gg} = 24, \quad c_2^{gg} = 48, \quad c_3^{gg} = \frac{80}{3}. \quad (2.9)$$

The squared amplitude for the LO can be written as:

$$|M_{LO}^{gg}|^2 = \frac{256}{3} (|M_1^{gg}|^2 + |M_2^{gg}|^2) - \frac{32}{3} \cdot 2Re(M_1^{gg\dagger} \cdot M_2^{gg}). \quad (2.10)$$

Then the LO cross section for the subprocesses $q\bar{q}, gg \rightarrow t\bar{b}H^-$ can be obtained by using the following formula:

$$\hat{\sigma}_{LO}^{q\bar{q}, gg} = \int d\Phi_3 \sum |M_{LO}^{q\bar{q}, gg}|^2, \quad (2.11)$$

where $d\Phi_3$ is the three-particle phase space element. The summation is taken over the spins and colors of initial and final states, and the bar over the summation recalls averaging over the spins and colors of initial partons. The LO total cross section of $pp/p\bar{p} \rightarrow t\bar{b}H^- + X$ can be expressed as:

$$\sigma_{LO}(AB(pp, p\bar{p}) \rightarrow t\bar{b}H^- + X) = \sum_{ij=(u\bar{u}), (d\bar{d})}^{(gg)} \frac{1}{1 + \delta_{ij}} \int dx_A dx_B [G_{i/A}(x_A, \mu) G_{j/B}(x_B, \mu) \hat{\sigma}_{LO}^{ij}(x_A, x_B, \mu) + (A \leftrightarrow B)], \quad (2.12)$$

where x_A and x_B are defined as

$$x_A = \frac{p_1}{P_A}, x_B = \frac{p_2}{P_B}, \quad (2.13)$$

where P_A and P_B are the four-momenta of the corresponding protons or antiprotons. A and B represent the incoming colliding hadrons(proton/antiproton). $\hat{\sigma}_{LO}^{ij}(ij = u\bar{u}, d\bar{d}, gg)$ is the LO parton-level total cross section for incoming i and j partons. $G_{i/A(B)}$'s are the LO parton distribution functions (PDF) with parton $i(j)$ in a proton/antiproton.

3 NLO QCD Corrections in the MSSM

In the calculation of the NLO QCD corrections in the framework of the MSSM, we adopt the 't Hooft-Feynman gauge, and use dimensional regularization(DR) method in $D = 4 - 2\epsilon$ dimensions to isolate the ultraviolet(UV), infrared(IR) and collinear singularities. Renormalization and factorization are performed in the modified minimal subtraction(\overline{MS}) scheme. The NLO QCD corrections can be divided into two parts: the virtual corrections from one-loop diagrams, and the real gluon/light-quark emission corrections.

3.1 Virtual Corrections

The virtual NLO QCD corrections in the MSSM come from self-energy, vertex, box and pentagon diagrams. We plot some QCD one-loop pentagon diagrams in Fig.3 for demonstration. These corrections in the MSSM can be sorted into two parts. One is the so-called SM-like QCD correction part coming from the diagrams with gluon/quark loops, another is SUSY-QCD correction part arising from virtual gluino/squark exchange contributions. The amplitude for the virtual SM-like NLO QCD correction part contains both ultraviolet(UV) and soft/collinear infrared(IR) singularities, while the amplitude corresponding to the NLO SUSY-QCD diagrams contains only UV singularities.

In order to remove the UV divergences, we need to renormalize the strong coupling constant, the wave functions of the relevant fields and the masses of bottom-, top-quark. In our calculation we introduce the following counterterms.

$$m_t \rightarrow m_t + \delta m_t, \quad m_b \rightarrow m_b + \delta m_b$$

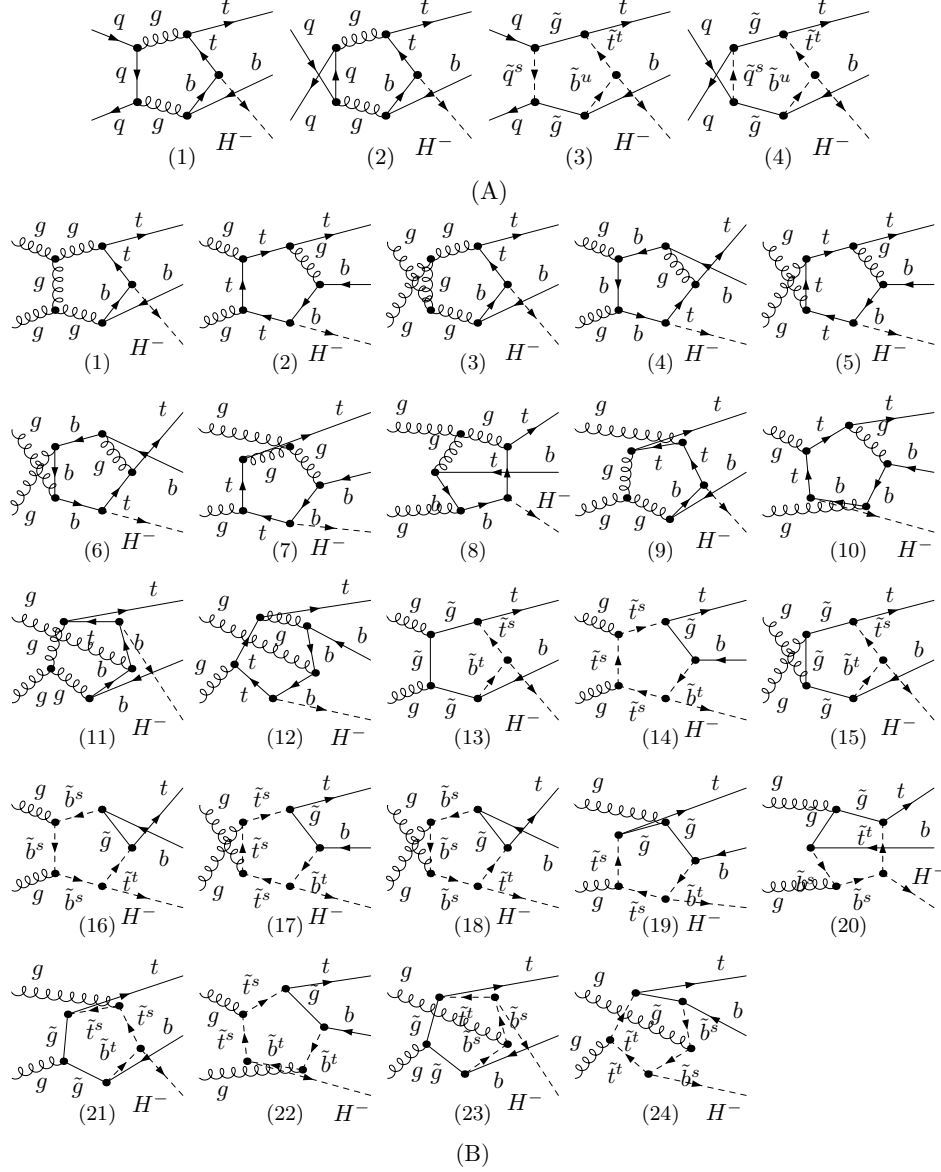


Fig. 3. (A) The QCD pentagon diagrams for the $q\bar{q} \rightarrow t\bar{t}H^-$ subprocess. (B) The QCD pentagon diagrams for the $gg \rightarrow t\bar{t}H^-$ subprocess.

$$\begin{aligned}
t_L &\rightarrow \left(1 + \frac{1}{2}\delta Z_L^t\right) t_L, & t_R &\rightarrow \left(1 + \frac{1}{2}\delta Z_R^t\right) t_R \\
b_L &\rightarrow \left(1 + \frac{1}{2}\delta Z_L^b\right) b_L, & b_R &\rightarrow \left(1 + \frac{1}{2}\delta Z_R^b\right) b_R \\
q_L &\rightarrow \left(1 + \frac{1}{2}\delta Z_L^q\right) q_L, & q_R &\rightarrow \left(1 + \frac{1}{2}\delta Z_R^q\right) q_R \\
G_\mu &\rightarrow \left(1 + \frac{1}{2}\delta Z_g\right) G_\mu, & g_s &\rightarrow g_s + \delta g_s
\end{aligned} \tag{3.1}$$

where g_s denotes the strong coupling constant, t , b , q , and G_μ denote the fields of top-, bottom-, up(down)-quark and gluon. The wave functions of the relevant fields, top quark mass in propagators and in the Yukawa couplings are renormalized in the on-shell(OS) scheme. For the renormalization of the strong coupling constant g_s , we adopt the \overline{MS} scheme at renormalization scale μ_r , except that the divergences associated with the top quark loop and colored SUSY particle loops are subtracted at zero momentum[20]. Since we define the counterterm of the strong coupling constant consisting of SM-like QCD term and SUSY QCD term($\delta g_s = \delta g_s^{(SM-like)} + \delta g_s^{(SQCD)}$), these two terms can be obtained as

$$\frac{\delta g_s^{(SM-like)}}{g_s} = -\frac{\alpha_s(\mu_r)}{4\pi} \left[\frac{\beta_0^{(SM-like)}}{2} \frac{1}{\bar{\epsilon}} + \frac{1}{3} \ln \frac{m_t^2}{\mu_r^2} \right], \tag{3.2}$$

$$\frac{\delta g_s^{(SQCD)}}{g_s} = -\frac{\alpha_s(\mu_r)}{4\pi} \left[\frac{\beta_1^{(SQCD)}}{2} \frac{1}{\bar{\epsilon}} + \frac{N}{3} \ln \frac{m_{\tilde{g}}^2}{\mu_r^2} + \sum_{U=u,c,t}^{i=1,2} \frac{1}{12} \ln \frac{m_{\tilde{U}_i}^2}{\mu_r^2} + \sum_{D=d,s,b}^{j=1,2} \frac{1}{12} \ln \frac{m_{\tilde{D}_j}^2}{\mu_r^2} \right], \tag{3.3}$$

where we have used the definitions:

$$\beta_0^{(SM-like)} = \frac{11}{3}N - \frac{2}{3}n_{lf} - \frac{2}{3}, \quad \beta_0^{(SQCD)} = -\frac{2}{3}N - \frac{1}{3}(n_{lf} + 1), \tag{3.4}$$

The number of colors $N = 3$, the number of light flavors $n_{lf} = 5$ and $1/\bar{\epsilon} = 1/\epsilon_{UV} - \gamma_E + \ln(4\pi)$. The summation is taken over the indexes of squarks and generations. Since the \overline{MS} scheme violates supersymmetry, it is necessary that the $q\tilde{q}\tilde{g}$ Yukawa coupling \hat{g}_s , which should be the same with the qqg gauge coupling g_s in the supersymmetry, takes a finite shift at one-loop order as shown in Eq.(3.5) [25]:

$$\hat{g}_s = g_s \left[1 + \frac{\alpha_s}{8\pi} \left(\frac{4}{3}N - C_F \right) \right], \tag{3.5}$$

with $C_F = 4/3$. In our numerical calculation we take this shift between \hat{g}_s and g_s into account.

In the Yukawa couplings, we use the \overline{MS} mass of the bottom quark, $\overline{m}_b(\mu_r)$, to absorb the large logarithms which arise from the renormalization of bottom quark mass[21], but keep the bottom quark

pole mass everywhere else. The bottom quark mass in propagators is renormalized by adopting the on-shell(OS) scheme. The expressions of the \overline{MS} mass of the bottom quark $\overline{m}_b(\mu_r)$ corresponding to 1-loop and 2-loop renormalization groups are given by:

$$\overline{m}_b(\mu_r)_{1-loop} = m_b \left[\frac{\alpha_s(\mu_r)}{\alpha_s(m_b)} \right]^{c_0/b_0}, \quad (3.6)$$

$$\overline{m}_b(\mu_r)_{2-loop} = m_b \left[\frac{\alpha_s(\mu_r)}{\alpha_s(m_b)} \right]^{c_0/b_0} \left[1 + \frac{c_0}{b_0} (c_1 - b_1) \frac{\alpha_s(\mu_r) - \alpha_s(m_b)}{\pi} \right] \left(1 - \frac{4}{3} \frac{\alpha_s(m_b)}{\pi} \right), \quad (3.7)$$

where

$$b_0 = \frac{1}{4\pi} \left(\frac{11}{3}N - \frac{2}{3}n_{lf} \right), \quad c_0 = \frac{1}{\pi}, \quad (3.8)$$

$$b_1 = \frac{1}{2\pi} \frac{51N - 19n_{lf}}{11N - 2n_{lf}}, \quad c_1 = \frac{1}{72\pi} (101N - 10n_{lf}), \quad (3.9)$$

The renormalization of the bottom quark mass in Yukawa couplings is defined as:

$$m_b^0 = \overline{m}_b(\mu_r) [1 + \delta^{QCD} + \delta^{SQCD}], \quad (3.10)$$

where the counterterm for the SM-like QCD δ^{QCD} is calculated in \overline{MS} scheme, while SUSY-QCD counterterm δ^{SQCD} is calculated in on-shell(OS) scheme.

Since there are significant corrections to $t\bar{b}H^-$ production for large values of $\tan\beta$, we absorb these corrections in the Yukawa couplings[22]. The resummed $t\bar{b}H^-$ Yukawa coupling can be expressed as:

$$\tilde{g}_{t\bar{b}H^-} = \frac{\sqrt{2}}{v} \left\{ m_t \cot\beta P_R + \overline{m}_b(\mu_r) \tan\beta P_L \frac{1 - \frac{\Delta_b}{\tan^2\beta}}{1 + \Delta_b} \right\}, \quad (3.11)$$

where [23]

$$\begin{aligned} \Delta_b &= \frac{\Delta m_b}{1 + \Delta_1}, \\ \Delta m_b &= \frac{2}{3} \frac{\alpha_s}{\pi} m_{\tilde{g}} \mu \tan\beta I(m_{\tilde{b}_1}^2, m_{\tilde{b}_2}^2, m_{\tilde{g}}^2), \\ \Delta_1 &= -\frac{2}{3} \frac{\alpha_s}{\pi} m_{\tilde{g}} A_b I(m_{\tilde{b}_3}^2, m_{\tilde{b}_2}^2, m_{\tilde{g}}^2), \\ I(a, b, c) &= -\frac{ab \log \frac{a}{b} + bc \log \frac{b}{c} + ca \log \frac{c}{a}}{(a-b)(b-c)(c-a)}. \end{aligned} \quad (3.12)$$

When we use the resummed $t\bar{b}H^-$ Yukawa coupling to express the tree-level cross sections, we have to add a finite renormalization of the bottom quark mass in $t\bar{b}H^-$ Yukawa coupling to avoid double

counting in the NLO QCD cross section. [24]:

$$\begin{aligned} m_b &\rightarrow \bar{m}_b(\mu_r) \left[1 + \Delta_b^{H^-} \right] + \mathcal{O}(\alpha_s^2), \\ \Delta_b^{H^-} &= \frac{2}{3} \frac{\alpha_s}{\pi} \left(1 + \frac{1}{\tan^2 \beta} \right) m_{\tilde{g}} \mu \tan \beta I(m_{\tilde{b}_1}^2, m_{\tilde{b}_2}^2, m_{\tilde{g}}^2). \end{aligned}$$

In the calculations of one-loop diagrams we adopt the definitions of one-loop integral functions as in Ref.[26]. The Feynman diagrams and the relevant amplitudes are generated by using *FeynArts* 3[27], and the Feynman amplitudes are subsequently reduced by *FormCalc32*[28]. The phase space integration is implemented by using Monte Carlo technique. For the IR-finite integral functions, the numerical calculations are implemented by using developed *LoopTools*[29].

The numerical calculations of the IR-infinite integral functions are implemented by using the methods described in Ref. [30]. The method is given by:

$$T_{\mu_1 \dots \mu_P}^{(N)D} = T_{\mu_1 \dots \mu_P}^{(N)D}|_{sing} + T_{\mu_1 \dots \mu_P}^{(N)4} - T_{\mu_1 \dots \mu_P}^{(N)4}|_{sing}, \quad (3.13)$$

where $T_{\mu_1 \dots \mu_P}^{(N)D}$ and $T_{\mu_1 \dots \mu_P}^{(N)D}|_{sing}$ are the N -point integral functions and their complete mass-singular parts in $D = 4 - 2\epsilon$ dimensions, respectively. $T_{\mu_1 \dots \mu_P}^{(N)4}$ and $T_{\mu_1 \dots \mu_P}^{(N)4}|_{sing}$ are in 4 dimensions. $T_{\mu_1 \dots \mu_P}^{(N)4}$ can be calculated by using mass renormalization scheme. $T_{\mu_1 \dots \mu_P}^{(N)}|_{sing}$ can be calculated by:

$$\begin{aligned} T_{\mu_1 \dots \mu_P}^{(N)}(p_0, \dots, p_{N-1}, m_0, \dots, m_{N-1})|_{sing} = \\ \sum_{n=0}^{N-1} \sum_{\substack{k=0 \\ k \neq n, n+1}}^{N-1} A_{nk} C_{\mu_1 \dots \mu_P}(p_n, p_{n+1}, p_k, m_n, m_{n+3}, m_k). \end{aligned} \quad (3.14)$$

where $C_{\mu_1 \dots \mu_P}$ is the corresponding 3-point integral functions. $C_{\mu_1 \dots \mu_P}$ in 4 dimensions can be calculated by using mass renormalization scheme. The explicit expressions of the $L_{\mu_1 \dots \mu_P}$ in $D = 4 - 2\epsilon$ dimensions can be found in Ref.[31].

The $\mathcal{O}(\alpha_s)$ QCD virtual corrections of the cross sections in the MSSM to the subprocesses $q\bar{q}, gg \rightarrow t\bar{t}h^0$ can be expressed as

$$\hat{\sigma}_{virtual}^{(q\bar{q}, gg)} = \int d\Phi_3 \overline{\sum} 2\text{Re} \left(\mathcal{M}_{tree}^{(q\bar{q}, gg)} \mathcal{M}_{virtual}^{(q\bar{q}, gg)\dagger} \right), \quad (3.15)$$

where $\mathcal{M}_{tree}^{(q\bar{q})}$ and $\mathcal{M}_{tree}^{(gg)}$ are the Born amplitudes for $q\bar{q}, gg \rightarrow t\bar{t}h^0$ subprocesses, and $\mathcal{M}_{virtual}^{(q\bar{q})}$ and $\mathcal{M}_{virtual}^{(gg)}$ are the renormalized amplitudes of all the NLO QCD Feynman diagrams involving virtual gluon/quark and gluino/squark for $q\bar{q}$ annihilation and gg fusion processes, respectively.

Then the $\hat{\sigma}_{virtual}$ is UV finite, but still has IR divergence. Its soft IR divergence part can be cancelled by adding with the soft real gluon emission corrections, and the remaining collinear divergences are absorbed into the parton distribution functions.

3.2 Real Parton Emission Corrections

The $\mathcal{O}(\alpha_s)$ corrections due to real parton emission give the origin of IR singularities. These singularities can be either of soft or collinear nature and can be conveniently isolated by slicing the phase space into different regions defined with suitable cutoffs, a method which has a general name of phase space slicing(PSS)[32]. In our calculation we consider the real parton emission subprocesses listed below for a consistent and complete mass factorization:

$$\begin{aligned}
q(p_1) + \bar{q}(p_2) &\rightarrow t(p_3) + \bar{b}(p_4) + H^-(p_5) + g(p_6), \\
g(p_1) + g(p_2) &\rightarrow t(p_3) + \bar{b}(p_4) + H^-(p_5) + g(p_6), \\
(q, \bar{q})(p_1) + g(p_2) &\rightarrow t(p_3) + \bar{b}(p_3) + H^-(p_5) + (q, \bar{q})(p_6), \quad (q = u, d).
\end{aligned} \tag{3.16}$$

Using the method of phase space slicing method[32], we introduce an arbitrary small soft cutoff δ_s to separate the $2 \rightarrow 4$ phase space into two regions, according to whether the energy of the emitted gluon is soft, i.e. $E_6 \leq \delta_s \sqrt{\hat{s}}/2$, or hard, i.e. $E_6 > \delta_s \sqrt{\hat{s}}/2$. In the real gluon emission processes $q\bar{q} \rightarrow t\bar{b}H^-g$ and $gg \rightarrow t\bar{b}H^-g$, there are both soft and collinear IR singularities. While in the real light-quark emission processes (in (3.16)), there are only collinear IR singularities, but no soft ID singularity. The cross sections for the real gluon emission subprocesses listed in (3.16) can be divided into two parts to isolate the soft IR singularities:

$$\begin{aligned}
\hat{\sigma}_{real}(q\bar{q}, gg \rightarrow t\bar{b}H^-g) &= \hat{\sigma}_{soft}(q\bar{q}, gg \rightarrow t\bar{b}H^-g) \\
&+ \hat{\sigma}_{hard}(q\bar{q}, gg \rightarrow t\bar{b}H^-g),
\end{aligned} \tag{3.17}$$

where $\hat{\sigma}_{soft}$ is obtained by integrating over the soft region of the emitted gluon phase space, and contains all the soft IR singularities. Furthermore, we decompose $\hat{\sigma}_{hard}$ of the four subprocesses (in (3.16)) with real gluon/light-quark emission, into a sum of hard-collinear (MC) and hard-non-collinear (\overline{HC}) terms to isolate the remaining collinear singularities from $\hat{\sigma}_{hard}$, by introducing another cutoff δ_c named collinear cutoff, i.e.,

$$\begin{aligned}
\hat{\sigma}_{hard}(q\bar{q}, gg, qq, \bar{q}g \rightarrow t\bar{b}H^-(g, g, q, \bar{q})) &= \hat{\sigma}_{HC}(q\bar{q}, gg, qq, \bar{q}g \rightarrow t\bar{b}H^-(g, g, q, \bar{q})) \\
&+ \hat{\sigma}_{\overline{HC}}(q\bar{q}, gg, qq, \bar{q}g \rightarrow t\bar{b}H^-(g, g, q, \bar{q})).
\end{aligned} \tag{3.18}$$

In the HC regions of the phase space the following collinear conditions are satisfied:

$$\frac{2p_1 \cdot p_6}{E_6 \sqrt{\hat{s}}} < \delta_c \quad or \quad \frac{2p_2 \cdot p_6}{E_6 \sqrt{\hat{s}}} < \delta_c, \tag{3.19}$$

and at the same time the emitted parton remains hard. $\hat{\sigma}_{HC}$ contains the collinear divergences. The analytical expressions of the cross sections in the soft and HC region, $\hat{\sigma}_{soft}$ and $\hat{\sigma}_{HC}$, can be obtained

by performing the phase space integration in d -dimension. In the \overline{HC} region, $\hat{\sigma}_{\overline{HC}}$ is finite and can be evaluated by using standard Monte Carlo techniques in 4-dimensions [34]. The cross sections of the real gluon emission process $pp/p\bar{p} \rightarrow t\bar{b}H^-g + X$, σ_{soft} , σ_{HC} and $\sigma_{\overline{HC}}$, depend on the two arbitrary parameters, δ_s and δ_c . However, after mass factorization the total NLO QCD corrected cross section $\sigma_{real}(pp/p\bar{p} \rightarrow t\bar{b}H^-g + X)$ is independent on these two arbitrary cutoffs. We shall explicitly discuss that in Sec.4. This constitutes an important check of our calculation. In the next two subsections, we will discuss in detail about the soft and hard-collinear gluon emission.

3.2.1 Soft Gluon Emission

For the real gluon emission subprocesses

$$q(p_1)\bar{q}(p_2) \rightarrow t(p_3)\bar{b}(p_4)H^-(p_5)g(p_6), \quad g(p_1)g(p_2) \rightarrow t(p_3)\bar{b}(p_4)H^-(p_5)g(p_6) \quad (3.20)$$

the soft region of the phase space is defined by

$$0 < E_6 \leq \delta_s \sqrt{\hat{s}}/2. \quad (3.21)$$

The gluon bremsstrahlung cross sections of both $q\bar{q}$ and gg collision channels can be written in the following form[19]:

$$\hat{\sigma}_{soft} = \hat{\sigma}_{LO} \otimes \frac{\alpha_s}{2\pi} \sum_{\substack{i,j=1 \\ i < j}}^4 (\mathbf{T}_i \cdot \mathbf{T}_j) g_{ij}(p_i, p_j), \quad (3.22)$$

where \mathbf{T}_i are the color operators [19, 36, 37], g_{ij} are the soft integrals defined as:

$$g_{ij}(p_i, p_j) = \frac{(2\pi\mu)^{2\epsilon}}{2\pi} \int_{E_6 \leq \delta_s \sqrt{\hat{s}}/2} \frac{d^{D-1}\mathbf{p}_6}{E_6} \left[\frac{2(p_i p_j)}{(p_i p_6)(p_j p_6)} - \frac{p_i^2}{(p_i p_6)^2} - \frac{p_j^2}{(p_j p_6)^2} \right]. \quad (3.23)$$

The similar expressions of the soft integrals for $q\bar{q}, gg \rightarrow t\bar{t}H^0$ in the SM can be found in Ref [18, 19].

Using the definitions of color operators, we get the expressions of $\hat{\sigma}_{soft}$ for $q\bar{q}$ annihilation and gg fusion channels, respectively.

$$\hat{\sigma}_{soft}^{q\bar{q}} = -\frac{\alpha_s}{2\pi} \left[\frac{1}{6}(g_{12} + g_{34}) - \frac{7}{6}(g_{13} + g_{24}) - \frac{1}{3}(g_{14} + g_{23}) \right] \hat{\sigma}_{LO}^{q\bar{q}}, \quad (3.24)$$

$$\begin{aligned} \hat{\sigma}_{soft}^{gg} = & \frac{\alpha_s}{12\pi} \int d\Phi_3 \sum \left[\left(\frac{256}{3} D_1 + 16 D_3 \right) |M_1^{gg}|^2 + \left(\frac{256}{3} D_2 + 16 D_4 \right) |M_2^{gg}|^2 \right. \\ & \left. + \left(-\frac{32}{3} D_1 + 16 D_3 \right) 2 \text{Re}(M_1^{gg\dagger} \cdot M_2^{gg}) \right], \end{aligned} \quad (3.25)$$

where M_1^{gg} and M_2^{gg} have been expressed in Eqs.(2.7) and (2.8) respectively, and the notations, D_1 , D_2 , D_3 , and D_4 , used in above equation are defined as

$$\begin{aligned} D_1 &= 9g_{12} + 9g_{13} + 9g_{24} - g_{34}, \\ D_2 &= 9g_{12} + 9g_{23} + 9g_{14} - g_{34}, \\ D_3 &= 6(g_{12} - g_{14} - g_{23} + g_{34}), \\ D_4 &= 6(g_{12} - g_{13} - g_{24} + g_{34}), \end{aligned} \quad (3.26)$$

3.2.2 Collinear Parton Emission from the Initial Parton

9. Hard Gluon Emission Subprocess $q\bar{q}(gg) \rightarrow t\bar{b}H^-g$

Let the hard gluon be emitted collinear to one of the incoming partons, i.e.,

$$\frac{2p_1 \cdot p_6}{E_6 \sqrt{\hat{s}}} < \delta_c, \quad \text{or} \quad \frac{2p_2 \cdot p_6}{E_6 \sqrt{\hat{s}}} < \delta_c. \quad (3.27)$$

In this region, one of the initial state partons, $i(i = q, \bar{q}, g)$, is considered to split into a hard parton i' and a collinear gluon, i.e., $i \rightarrow i'g$, with $p_{i'} = zp_i$ and $p_6 = (1 - z)p_i$. The matrix element squared for $q\bar{q}(gg) \rightarrow t\bar{b}H^-g$ factorizes into the Born matrix element squared and the Altarelli-Parisi splitting function, and is expressed as:

$$\overline{\sum} |M_{HC}(ij \rightarrow t\bar{b}H^-g)|^2 \simeq (4\pi\alpha_s\mu_r^{2\epsilon}) \overline{\sum} |M_{LO}(i'j \rightarrow t\bar{b}H^-g)|^2 \left(\frac{-2P_{ii'}(z, \epsilon)}{z\hat{t}_{i6}} \right), \quad (3.28)$$

where

$$\begin{aligned} P_{ii'}(z, \epsilon) &= P_{ii'}(z) + \epsilon P'_{ii'}(z), \\ P_{gg}(z) &= 2N \left[\frac{z}{1-z} + \frac{1-z}{z} + z(1-z) \right], \quad P'_{gg}(z) = 0, \\ P_{qq}(z) &= C_F \left(\frac{1+z^2}{1-z} \right), \quad P'_{qq}(z) = -C_F(1-z). \end{aligned} \quad (3.29)$$

Using the approximation $p_i - p_6 \simeq zp_i (i = 1, 2)$, the element in the four body collinear phase space region can be written as[18]

$$d\Phi_4|_{coll} = d\Phi_3 \frac{(4\pi)^\epsilon}{16\pi^2\Gamma(1-\epsilon)} z dz d\hat{t}_{i6} [-(1-z)\hat{t}_{i6}]^{-\epsilon} \theta \left(\frac{(1-z)}{z} s' \frac{\delta_c}{2} - s_{i6} \right), \quad (i = 1, 2), \quad (3.30)$$

where $s' = 2p_{i'} \cdot p_j$. Note that the four body phase space should be evaluated at a squared parton-parton energy of $z\hat{s}$. Therefore, after integration over the collinear gluon degrees of freedom, we

obtain[33]

$$\begin{aligned}\hat{\sigma}_{HC} &= \left[\frac{\alpha_s}{2\pi} \frac{\Gamma(1-\epsilon)}{\Gamma(1-2\epsilon)} \left(\frac{4\pi\mu_r^2}{s'} \right)^\epsilon \right] \left(-\frac{1}{\epsilon} \right) \delta_c^{-\epsilon} \\ &\times \left\{ \int_0^{1-\delta_s} dz \left[\frac{(1-z)^2}{2z} \right]^{-\epsilon} P_{ii'}(z, \epsilon) \hat{\sigma}_{LO}(i'j \rightarrow t\bar{b}H^-) + (i \leftrightarrow j) \right\}.\end{aligned}\quad (3.31)$$

In order to factorize the collinear singularity into the parton distribution function, we introduce a scale dependent parton distribution function using the \overline{MS} convention:

$$\begin{aligned}G_{q/A}(x, \mu_f) &= G_{q/A}(x) \left[1 - \frac{\alpha_s}{2\pi} \frac{\Gamma(1-\epsilon)}{\Gamma(1-2\epsilon)} \left(\frac{4\pi\mu_r^2}{\mu_f^2} \right)^\epsilon \left(\frac{1}{\epsilon} \right) A_1^{sc}(q \rightarrow qq) \right] \\ &+ \left(-\frac{1}{\epsilon} \right) \left[\frac{\alpha_s}{2\pi} \frac{\Gamma(1-\epsilon)}{\Gamma(1-2\epsilon)} \left(\frac{4\pi\mu_r^2}{\mu_f^2} \right)^\epsilon \right] \int_x^{1-\delta_s} \frac{dz}{z} P_{qq}(z, \epsilon) G_{q/A}(x/z),\end{aligned}\quad (3.32)$$

$$\begin{aligned}G_{g/A}(x, \mu_f) &= G_{g/A}(x) \left[1 - \frac{\alpha_s}{2\pi} \frac{\Gamma(1-\epsilon)}{\Gamma(1-2\epsilon)} \left(\frac{4\pi\mu_r^2}{\mu_f^2} \right)^\epsilon \left(\frac{1}{\epsilon} \right) A_1^{sc}(g \rightarrow gg) \right] \\ &+ \left(-\frac{1}{\epsilon} \right) \left[\frac{\alpha_s}{2\pi} \frac{\Gamma(1-\epsilon)}{\Gamma(1-2\epsilon)} \left(\frac{4\pi\mu_r^2}{\mu_f^2} \right)^\epsilon \right] \int_x^{1-\delta_s} \frac{dz}{z} P_{gg}(z, \epsilon) G_{g/A}(x/z), \quad (A = p, \bar{p})\end{aligned}\quad (3.33)$$

where

$$\begin{aligned}A_1^{sc}(q \rightarrow qq) &= C_F(2 \ln \delta_s + 3/2), \quad C_F = 4/3, \\ A_1^{sc}(g \rightarrow gg) &= 2N \ln \delta_s + (11N - 2n_{lf})/6.\end{aligned}\quad (3.34)$$

By using above expressions, the NLO QCD correction parts of the total cross sections contributed by $q\bar{q}$ annihilation and gg fusion subprocesses in the initial state collinear phase space region are obtained as

$$\begin{aligned}\sigma_{HC}^{qq} &= \int \hat{\sigma}_{LO}^{qq} \left[\frac{\alpha_s}{2\pi} \frac{\Gamma(1-\epsilon)}{\Gamma(1-2\epsilon)} \left(\frac{4\pi\mu_r^2}{\hat{s}} \right)^\epsilon \right] \left\{ \tilde{G}_{q/A}(x_A, \mu_f) G_{\bar{q}/B}(x_B, \mu_f) + G_{\bar{q}/A}(x_A, \mu_f) \tilde{G}_{q/B}(x_B, \mu_f) \right. \\ &+ \left. \sum_{\alpha=u, \bar{u}}^{d, \bar{d}} \left[\frac{A_1^{sc}(\alpha \rightarrow \alpha g)}{\epsilon} + A_0^{sc}(\alpha \rightarrow \alpha g) \right] G_{q/A}(x_A, \mu_f) G_{\bar{q}/B}(x_B, \mu_f) + (A \leftrightarrow B) \right\} dx_A dx_B\end{aligned}\quad (3.35)$$

$$\begin{aligned}\sigma_{HC}^{gg} &= \int \hat{\sigma}_{LO}^{gg} \left[\frac{\alpha_s}{2\pi} \frac{\Gamma(1-\epsilon)}{\Gamma(1-2\epsilon)} \left(\frac{4\pi\mu_r^2}{\hat{s}} \right)^\epsilon \right] \frac{1}{2} \left\{ \tilde{G}_{g/A}(x_A, \mu_f) G_{g/B}(x_B, \mu_f) + G_{g/A}(x_A, \mu_f) \tilde{G}_{g/B}(x_B, \mu_f) \right. \\ &+ \left. \left[\frac{A_1^{sc}(g \rightarrow gg)}{\epsilon} + A_0^{sc}(g \rightarrow gg) \right] G_{g/A}(x_A, \mu_f) G_{g/B}(x_B, \mu_f) + (A \leftrightarrow B) \right\} dx_A dx_B,\end{aligned}\quad (3.36)$$

where

$$A_0^{sc} = A_1^{sc} \ln \left(\frac{\hat{s}}{\mu_f^2} \right),$$

$$\tilde{G}_{\alpha/A,B}(x, \mu_f) = \int_x^{1-\delta_s} \frac{dy}{y} G_{\alpha/A,B}(x/y, \mu_f) \tilde{P}_{\alpha\alpha}(y), \quad (\alpha = u, \bar{u}, d, \bar{d}, g), \quad (3.37)$$

with

$$\tilde{P}_{\alpha\alpha}(y) = P_{\alpha\alpha}(y) \ln \left(\frac{\delta_c}{2} \frac{(1-y)^2}{y} \frac{\hat{s}}{\mu_f^2} \right) - P'_{\alpha\alpha}(y), \quad (\alpha = u, \bar{u}, d, \bar{d}, g). \quad (3.38)$$

2. Hard Light-quark Emission Subprocesses $(q, \bar{q})g \rightarrow t\bar{b}H^- + (q, \bar{q})$

The method in the calculation of the hard light-quark emission subprocesses $(q, \bar{q})g \rightarrow t\bar{b}H^- + (q, \bar{q})$ is similar to that for hard gluon emission subprocesses. In the collinear region, the initial state parton $i (i = u, d, \bar{u}, \bar{d}, g)$ is considered to split into a hard parton i' and a collinear light-quark, $i \rightarrow i'q$, with $p_{i'} = zp_i$ and $p_6 = (1-z)p_i$. Let the hard light-quark be emitted collinear to one of the incoming partons, the collinear region is then defined as:

$$\frac{2p_1 \cdot p_6}{E_6 \sqrt{\hat{s}}} < \delta_c \quad \text{or} \quad \frac{2p_2 \cdot p_6}{E_6 \sqrt{\hat{s}}} < \delta_c. \quad (3.39)$$

The collinear singularity of $\hat{\sigma}_{real}^{qq}$ can be written as:

$$\begin{aligned} \hat{\sigma}_{HC}^{qq} &= \left[\frac{\alpha_s}{2\pi} \frac{\Gamma(1-\epsilon)}{\Gamma(1-2\epsilon)} \left(\frac{4\pi\mu_r^2}{s'} \right)^\epsilon \right] \left(-\frac{1}{\epsilon} \right) \delta_c^{-\epsilon} \left\{ \int_0^{1-\delta_s} dz \left[\frac{(1-z)^2}{2z} \right]^{-\epsilon} \right. \\ &\quad \times P_{qg}(z, \epsilon) \hat{\sigma}_{LO}^{gg}(gg \rightarrow t\bar{b}H^-) + P_{gq}(z, \epsilon) \hat{\sigma}_{LO}^{qq}(q\bar{q} \rightarrow t\bar{b}H^-) \left. \right\}. \end{aligned} \quad (3.40)$$

with

$$\begin{aligned} P_{ii'}(z, \epsilon) &= P_{ii'}(z) + \epsilon P'_{ii'}(z), \\ P_{gq}(z) &= \frac{1}{2} [z^2 + (1-z)^2], \quad P'_{gq}(z) = -z(1-z), \\ P_{qq}(z) &= \frac{N^2-1}{2N} \left(\frac{1+(1-z)^2}{z} \right), \quad P'_{qq}(z) = -\frac{N^2-1}{2N} z. \end{aligned} \quad (3.41)$$

Using the \overline{MS} scheme, the scale dependent distribution function can be written as:

$$G_{i'/A}(x, \mu_f) = G_{i'/A}(x) + \left(-\frac{1}{\epsilon} \right) \left[\frac{\alpha_s}{2\pi} \frac{\Gamma(1-\epsilon)}{\Gamma(1-2\epsilon)} \left(\frac{4\pi\mu_r^2}{\mu_f^2} \right)^\epsilon \right] \int_x^1 \frac{dz}{z} P_{ii'}(z) G_{i/A}(x/z). \quad (3.42)$$

And we can get the expression for the initial state collinear contribution at $O(\alpha_s)^3$ order:

$$\begin{aligned}
\sigma_{HC}^{qq} = & \frac{\alpha_s}{2\pi} \sum_{i=q,\bar{q}} \int dx_A dx_B \left\{ \int_{x_A}^1 \frac{dz}{z} G_{i/A}\left(\frac{x_A}{z}, \mu\right) G_{g/B}(x_B, \mu) \times \right. \\
& \hat{\sigma}_{LO}^{gg}(x_A, x_B, \mu) \left[P_{ig}(z) \ln \left(\frac{s}{\mu^2} \frac{(1-z)^2}{z} \frac{\delta_c}{2} \right) - P'_{ig}(z) \right] \\
& + \int_{x_A}^1 \frac{dz}{z} G_{g/A}\left(\frac{x_A}{z}, \mu\right) G_{i/B}(x_B, \mu) \times \\
& \left. \hat{\sigma}_{LO}^{q\bar{q}}(x_A, x_B, \mu) \left[P_{gi}(z) \ln \left(\frac{s}{\mu^2} \frac{(1-z)^2}{z} \frac{\delta_c}{2} \right) - P'_{gi}(z) \right] + (A \leftrightarrow B) \right\}. \quad (3.43)
\end{aligned}$$

3.3 Total NLO Cross Section

The final result for the $O(\alpha_s)$ NLO QCD corrected cross section part of qq annihilation subprocesses can be written as:

$$\begin{aligned}
\sigma_{NLO}^{qq} = & \int dx_A dx_B G_{q/A}(x_A, \mu) G_{\bar{q}/B}(x_B, \mu) \left[\hat{\sigma}_{LO}^{qq}(x_A, x_B, \mu) + \hat{\sigma}_{virtual}^{qq}(x_A, x_B, \mu) + \hat{\sigma}_{soft}^{qq}(x_A, x_B, \mu) \right. \\
& + (A \leftrightarrow B)] + \sigma_{HC}^{qq} + \int dx_A dx_B [G_{q/A}(x_A, \mu) G_{\bar{q}/B}(x_B, \mu) \hat{\sigma}_{HC}^{qq}(x_A, x_B, \mu) + (A \leftrightarrow B)]. \quad (3.44)
\end{aligned}$$

And the NLO QCD corrected cross section part for gg fusion subprocess has the expression as:

$$\begin{aligned}
\sigma_{NLO}^{gg} = & \frac{1}{2} \int dx_A dx_B G_{g/A}(x_A, \mu) G_{g/B}(x_B, \mu) [\hat{\sigma}_{LO}^{gg}(x_A, x_B, \mu) + \hat{\sigma}_{virtual}^{gg}(x_A, x_B, \mu) + \hat{\sigma}_{soft}^{gg}(x_A, x_B, \mu) \\
& + (A \leftrightarrow B)] + \sigma_{HC}^{gg} + \frac{1}{2} \int dx_A dx_B [G_{g/A}(x_A, \mu) G_{g/B}(x_B, \mu) \hat{\sigma}_{HC}^{gg}(x_A, x_B, \mu) + (A \leftrightarrow B)] \quad (3.45)
\end{aligned}$$

The cross section of $(q, \bar{q})g \rightarrow t\bar{b}H^- + (q, \bar{q})$ ($q = u, d$) can be written as:

$$\sigma_{NLO}^{qq} = \sigma_{HC}^{qq} + \sum_{i=q,\bar{q}} \int dx_A dx_B [G_{i/A}(x_A, \mu) G_{g/B}(x_B, \mu) \hat{\sigma}_{HC}^{qq}(x_A, x_B, \mu) + (A \leftrightarrow B)]. \quad (3.46)$$

with the hard-non-collinear partonic cross section given by

$$\hat{\sigma}_{HC}^{ij} = \int_{\overline{\text{HC}}} \overline{\sum} |M(ij \rightarrow t\bar{b}H^- g(q, \bar{q}))|^2 d\Phi_4. \quad (3.47)$$

where $d\Phi_4$ denotes the four-particle phase space element.

Finally, the NLO QCD corrected total cross sections for $pp/p\bar{p} \rightarrow t\bar{b}H^- + X$ can be obtain by using the formula:

$$\sigma_{NLO} = \sigma_{NLO}^{qq} + \sigma_{NLO}^{gg} + \sigma_{NLO}^{q\bar{q}}. \quad (3.48)$$

In our calculation, we have checked the cancellations of the UV and IR divergence analytically, and the final results are both UV- and IR-finite.

4 Numerical Results and Discussions

In our numerical calculation, we adopt the CTEQ6M[35] parton distribution functions and the 2-loop evolution of $\alpha_s(\mu)$ to evaluate the hadronic NLO QCD corrected cross sections with $\alpha_s^{NLO}(M_Z) = 0.118$, while for the hadronic LO cross sections we use the CTEQ6L1 parton distribution functions and the one-loop evolution of $\alpha_s(\mu)$. We take the SM parameters as: $\alpha_{ew}(M_Z)^{-1} = 127.918$, $m_W = 80.423 \text{ GeV}$, $m_Z = 91.18 \text{ GeV}$, $m_t = 175 \text{ GeV}$, $m_b = 4.62 \text{ GeV}$. As a numerical demonstration, in this work we refer to the Snowmass point SPS1b for the relevant MSSM parameters[38], if there is no other statement. The MSSM parameters in this benchmark are given by:

$$\begin{aligned} \tan \beta &= 30, & \mu &= 495.6 \text{ GeV}, & A_t &= -729.3 \text{ GeV}, \\ A_b &= -987.4 \text{ GeV}, & m_{\tilde{g}} &= 916.1 \text{ GeV}, & m_{\tilde{q}_L} &= 762.5 \text{ GeV}, \\ m_{\tilde{b}_R} &= 780.3 \text{ GeV}, & m_{\tilde{t}_R} &= 670.7 \text{ GeV}. \end{aligned} \quad (4.1)$$

The charged Higgs boson mass is taken as free parameter. The calculations are carrying out at the upgraded Tevatron with the $p\bar{p}$ colliding energy $\sqrt{s} = 2 \text{ TeV}$ and the LHC with pp colliding energy $\sqrt{s} = 14 \text{ TeV}$.

As the check of the correctness of our numerical calculation, we plot Fig.4 to show the dependence of σ_{real}^{gg} on δ_c and δ_s at the LHC. Fig.4(a) shows the σ_{real}^{gg} as the functions of δ_c by taking $\delta_s = 10^{-4}$, $m_{H^-} = 310 \text{ GeV}$ and δ_c varying from 10^{-6} to 10^{-4} . Fig.4(b) presents the curves of σ_{real}^{gg} versus δ_s with $\delta_c = 10^{-5}$, $m_{H^-} = 310 \text{ GeV}$ and δ_s running from 10^{-5} to 10^{-3} . Both figures show that our results of $\sigma_{real}^{gg}(gg \rightarrow t\bar{b}H^- + g)$ is independent of cutoff δ_c and δ_s . Actually, our calculation proves also that the real gluon emission cross section for $q\bar{q}$ annihilation channel is independent on cutoff δ_c and δ_s , and the cross sections for qg and $\bar{q}g$ fusion channels(as shown in (3.16)) are independent on δ_c too.

In following calculation, we require the final anti-bottom quark to have a transverse momentum(p_T^b) being larger than 20 GeV and a pseudorapidity $|\eta_b| \leq 2$ for the Tevatron and less than $|\eta_b| \leq 2.5$ for the LHC, unless other statement is given. We present the dependence of the cross section on the renormalization/factorization scale Q/Q_0 (where we take $Q \equiv \mu_r = \mu_f$ for simplicity and define $Q_0 = (m_t + m_{H^-} + m_b)/2$) in Fig.5(a1-a2) and Fig.5(b1-b2) taking $m_{H^-} = 175 \text{ GeV}$ at the Tevatron and $m_{H^-} = 250 \text{ GeV}$ at the LHC, separately. In Fig.5(a1) and Fig.5(b1) we depict the curves for total cross sections at leading-order σ_{LO} and σ_{NLO} including NLO corrections for the processes $p\bar{p}/pp \rightarrow t\bar{b}H^- + X$ at the Tevatron and the LHC. They show that the σ_{NLO} in the MSSM is less dependent on the normalization/factorization scale Q/Q_0 than σ_{LO} both at the Tevatron and the LHC, especially in Fig.5(b1) the curve for σ_{NLO} at the LHC is nearly independent of Q/Q_0 . We can see from Fig.5(a1) that the NLO QCD corrections suppress the LO cross section of the process $p\bar{p} \rightarrow t\bar{b}H^- + X$ at the Tevatron. Fig.5(a2) shows that at the Tevatron the dominant contribution to σ_{NLO} is from the subprocess $q\bar{q} \rightarrow t\bar{b}H^-$, while Fig.5(b2) demonstrates that the main contributions are coming from subprocess $gg \rightarrow t\bar{b}H^-$ at the LHC. From Fig.5(a1) we can see that if Q goes down to a very low value, i.e., $Q \ll Q_0$, the curve for σ_{NLO} tends to have a negative value. The reason is that

large logarithmic corrections spoil the convergence of perturbation theory in the proton-antiproton colliding energy at the Tevatron. From Fig.6(a1-a2) and (b1-b2), we conclude that the dependence of the NLO QCD corrected cross section σ_{NLO} on the scale Q is significantly reduced comparing with σ_{LO} , especially at the LHC, there the σ_{NLO} is very stable in a large range of Q .

In the following figures, we fix the value of the renormalization/factorization scale being $Q = Q_0 = \mu_r = \mu_f$. In Fig.6(a1) and (b1) we depict the LO and total NLO QCD corrected cross sections, σ_{LO} and σ_{NLO} , in the MSSM as the functions of m_{H^-} at the Tevatron and the LHC, respectively. The corresponding relative NLO QCD corrections $\delta(\equiv \frac{\sigma_{NLO}-\sigma_{LO}}{\sigma_{LO}})$ versus m_{H^-} are plotted in Fig.6(a2) and (b2), separately. From these figures, we can see that the cross sections σ_{NLO} and σ_{LO} decrease rapidly as m_{H^-} varies in the range from 175GeV to 300GeV at the Tevatron and from 175GeV to 550GeV at the LHC. We can read from Fig.6(a1) that when m_{H^-} increases from 175 GeV to 300 GeV , the total NLO QCD corrected cross section σ_{NLO} in the MSSM decreases from 0.66 fb to 0.02 fb at the Tevatron. From Fig.6(a2) we can read when m_{H^-} increases from 175 GeV to 550 GeV , σ_{NLO} decreases from 160 fb to 3 fb at the LHC. The absolute value of the relative correction δ in Fig.6(a2) decreases slightly from 39% to 32% at the Tevatron. While the absolute value of the relative correction δ in Fig.6(b2) increases rapidly with the increment of the charged Higgs boson mass at the LHC, it reaches the value of 44% when $m_{H^-} = 550\text{ GeV}$.

In Fig.7(a-b), we present the total LO and NLO QCD corrected cross sections σ_{LO} and σ_{NLO} in the MSSM as the functions of the transverse momentum of anti-bottom quark cut $p_{T,cut}^b$, taking $m_{H^-} = 175\text{ GeV}$ at the Tevatron and $m_{H^-} = 250\text{ GeV}$ at the LHC, respectively. In these two figures, we can see that the cross sections σ_{NLO} and σ_{LO} decrease as $p_{T,cut}^b$ goes up from 10 GeV to 25 GeV . We can read from Fig.7(a-b) that when $p_{T,cut}^b$ increases from 10 GeV to 25 GeV , the total NLO QCD corrected cross section σ_{NLO} in the MSSM decreases roughly from $0.87\text{ fb}(55\text{ fb})$ to $0.56\text{ fb}(37\text{ fb})$ for the Tevatron(LHC).

Fig.8(a1) and Fig.8(b1) show the LO and total NLO QCD corrected cross sections σ_{LO} and σ_{NLO} in the MSSM as the functions of $\tan\beta$ with $m_{H^-} = 175\text{ GeV}$ at the Tevatron and $m_{H^-} = 250\text{ GeV}$ at the LHC, respectively. When $\tan\beta$ has a small value, the NLO QCD corrected cross section decreases from $0.45\text{ fb}(30\text{ fb})$ to $0.15\text{ fb}(127\text{ fb})$ at the Tevatron(LHC), as $\tan\beta$ goes up from 4 to 12 . The NLO QCD corrected cross sections σ_{NLO} increases from $0.15\text{ fb}(12\text{ fb})$ to $2\text{ fb}(132\text{ fb})$ for the Tevatron(LHC), as $\tan\beta$ varies from 12 to 50 . The corresponding relative corrections δ are plotted in Fig.8(a2) and Fig.8(b2). The δ can be beyond -50% at the Tevatron, and approach -40% at the LHC at the position of $\tan\beta \sim 15$.

In Fig.9, we depict the distributions of the transverse momenta of the final states(p_T^b , p_T^t and $p_T^{H^-}$) with $m_{H^-} = 250\text{ GeV}$ at the LHC and $m_{H^-} = 175\text{ GeV}$ at the Tevatron, separately. In Fig.9(a1-a2, b1-b2, c1-c2), we show the distributions of the differential cross sections $d\sigma_{LO,NLO}/dp_T^b$, $d\sigma_{LO,NLO}/dp_T^t$ and $d\sigma_{LO,NLO}/dp_T^{H^-}$ at the LHC and the Tevatron, respectively. These figures demonstrate that the NLO QCD corrections significantly modify the leading-order distributions of the differential cross sections $d\sigma_{LO}/dp_T^b$, $d\sigma_{LO}/dp_T^t$ and $d\sigma_{LO}/dp_T^{H^-}$ at hadron colliders. We find that in the low p_T^b region the differential cross sections $d\sigma_{LO,NLO}/dp_T^b$ can be very large, especially at the LHC.

5 Summary

In this paper we calculated the NLO QCD corrections to the processes $p\bar{p}/pp \rightarrow t\bar{b}H^- + X$ in the MSSM at the Tevatron and the LHC. We investigated the contributions of the NLO QCD corrections to the total cross sections and the distributions of the transverse momenta of final particles(anti-bottom-quark, t-quark and charged Higgs-boson), and found the NLO QCD corrections significantly modify the corresponding LO differential cross sections. We analyzed the dependence of the NLO QCD corrected cross sections and the corresponding relative corrections on the renormalization/factorization scale Q , charged Higgs-boson mass m_{H^-} , transverse momentum cut of anti-bottom quark $p_{T,cut}^b$, and $\tan\beta$, respectively. Our numerical results show that the theoretical NLO QCD corrections in the MSSM reduce the dependence of the cross section on the factorization and normalization scales, especially the NLO QCD corrected total cross sections at the LHC are nearly independent of these scales, and the relative correction is obviously related to m_{H^-} and $\tan\beta$ at both the Tevatron and the LHC. We find the total NLO QCD relative corrections δ can be beyond -50% at the Tevatron and approach -40% at the LHC.

Acknowledgments This work was supported in part by the National Natural Science Foundation of China and special fund sponsored by China Academy of Science.

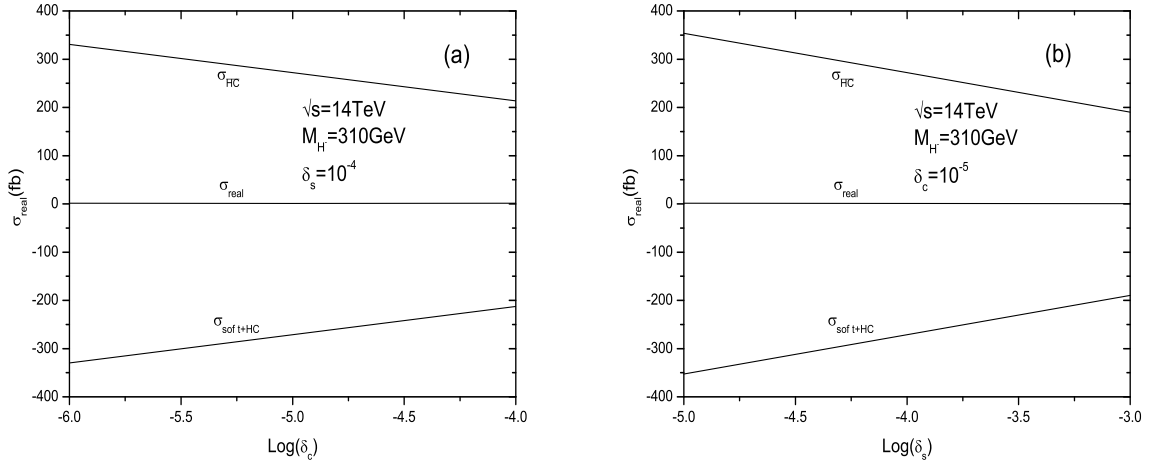


Fig. 4. The cutoff dependence of σ_{real}^{gg} with $M_{H^-} = 310 \text{ GeV}$ at the Snowmass point SPS1b at the LHC. Fig.4(a) shows the δ_c dependence with $\delta_s = 10^{-4}$, and Fig.4(b) shows the δ_s dependence with $\delta_c = 10^{-5}$.

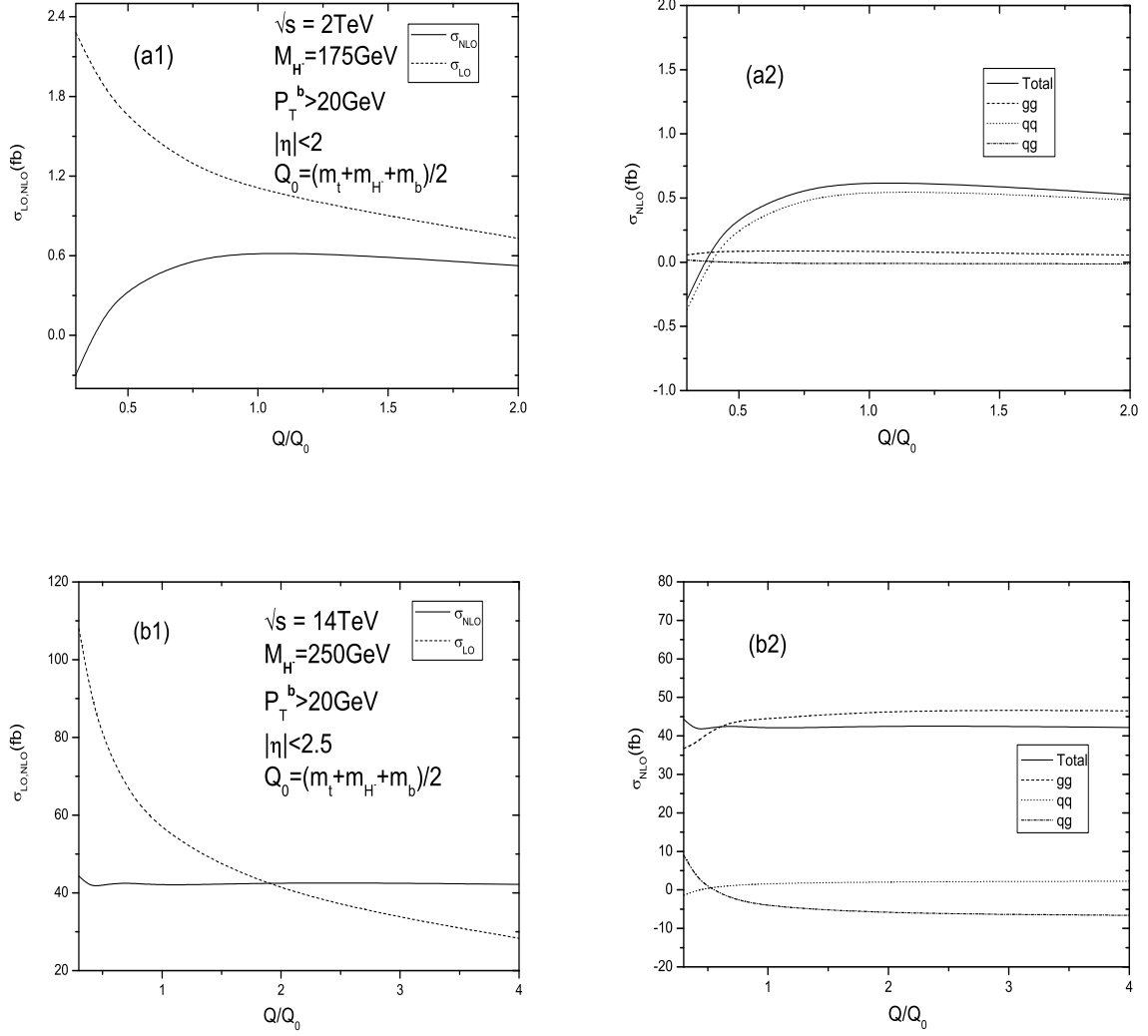


Fig. 5. The total cross sections σ_{LO} and σ_{NLO} for the processes $pp/p\bar{p} \rightarrow t\bar{t}H^- + X$ as the functions of the renormalization/factorization scale Q with $m_{H^-} = 175 \text{ GeV}$, $|\eta_b| \leq 2$ at the Tevatron and $m_{H^-} = 250 \text{ GeV}$, $|\eta_b| \leq 2.5$ at the LHC, are shown in Fig.5(a1) and Fig.5(b1) respectively. The contribution parts to the total cross sections $\sigma_{NLO}(pp/p\bar{p} \rightarrow t\bar{t}H^- + X)$ from the related qq , gg , qg fusion subprocesses as the functions of the renormalization/factorization scale Q with $m_{H^-} = 175 \text{ GeV}$ at the Tevatron and $m_{H^-} = 250 \text{ GeV}$ at the LHC, are shown in Fig.5(a2) and Fig.5(b2) separately.

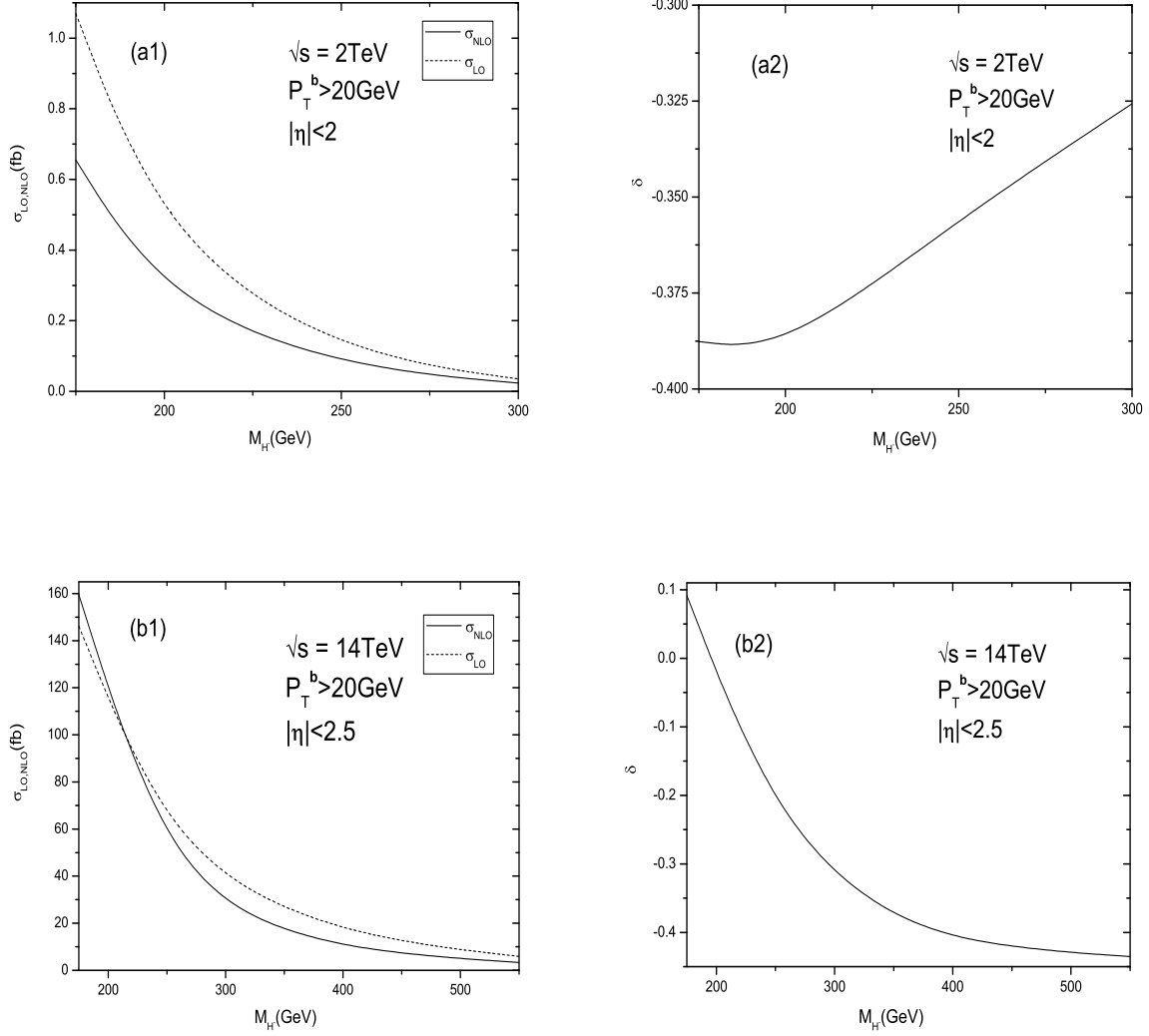


Fig. 6. The total NLO QCD corrected cross sections (σ_{NLO}) and the corresponding relative corrections(δ) of the processes $p\bar{p}/pp \rightarrow t\bar{b}H^- + X$ with $m_{H^-} = 175\text{ GeV}$, $|\eta_b| \leq 2$ at the Tevatron and $m_{H^-} = 250\text{ GeV}$, $|\eta_b| \leq 2.5$ at the LHC, as the functions of m_{H^-} . Fig.6(a1) and Fig.6(a2) are for the process $p\bar{p} \rightarrow t\bar{b}H^- + X$ at the Tevatron and Fig.6(b1) and Fig.6(b2) for the process $pp \rightarrow t\bar{b}H^- + X$ at the LHC.

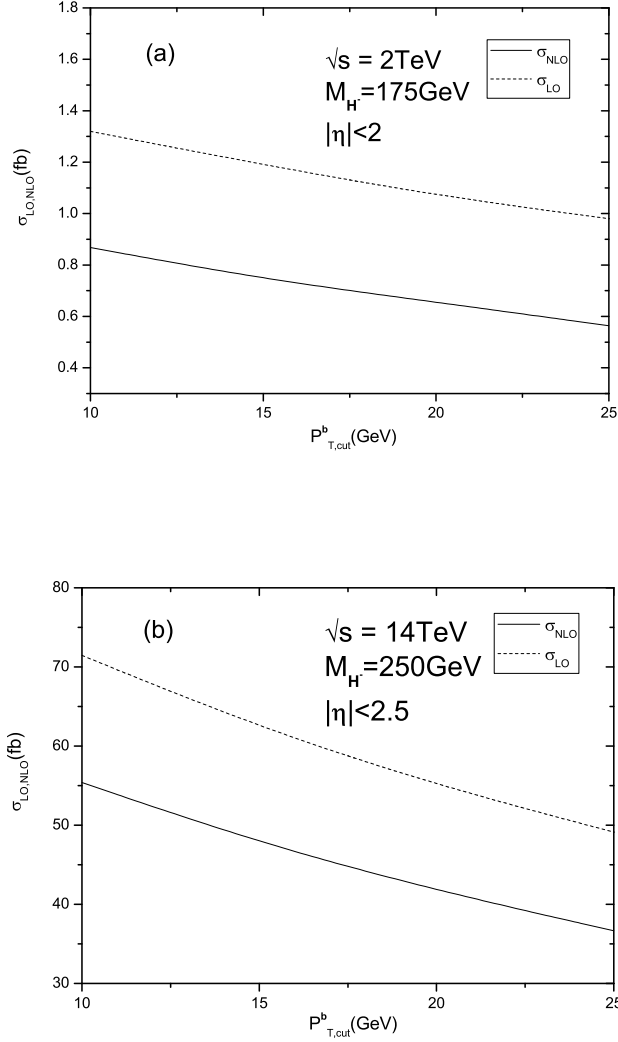


Fig. 7. The total NLO QCD corrected cross sections(σ_{NLO}) of the processes $p\bar{p}/pp \rightarrow t\bar{b}H^- + X$ at the Tevatron and the LHC, as the functions of the anti-bottom quark transverse momentum cut $p_{T,cut}^b$ with $m_{H^-} = 175\text{ GeV}$, $|\eta_b| \leq 2$ at the Tevatron and $m_{H^-} = 250\text{ GeV}$, $|\eta_b| \leq 2.5$ at the LHC. Fig.7(a) is for the process $p\bar{p} \rightarrow t\bar{b}H^- + X$ at the Tevatron and Fig.7(b) for the process $pp \rightarrow t\bar{b}H^- + X$ at the LHC.

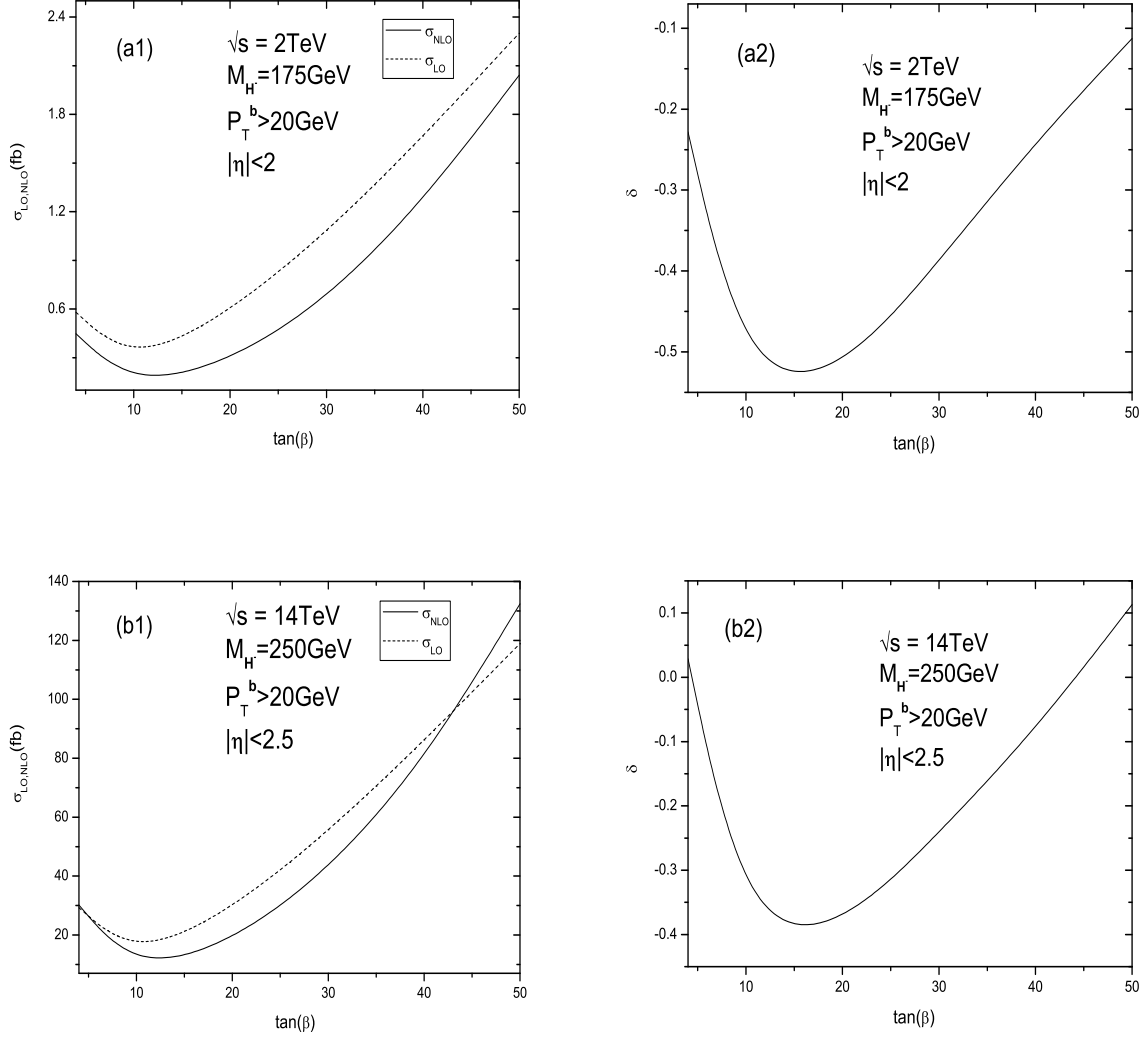


Fig. 8. The total NLO QCD corrected cross sections(σ_{NLO}) and the corresponding relative corrections(δ) of the processes $p\bar{p}/pp \rightarrow t\bar{b}H^- + X$ with $m_{H^-} = 175\text{ GeV}$, $|\eta_b| \leq 2$ at the Tevatron and $m_{H^-} = 250\text{ GeV}$, $|\eta_b| \leq 2.5$ at the LHC, as the functions of $\tan\beta$. Fig.8(a1) and Fig.8(a2) are for the process $p\bar{p} \rightarrow t\bar{b}H^- + X$ at the Tevatron and Fig.8(b1) and Fig.8(b2) for the process $pp \rightarrow t\bar{b}H^- + X$ at the LHC.

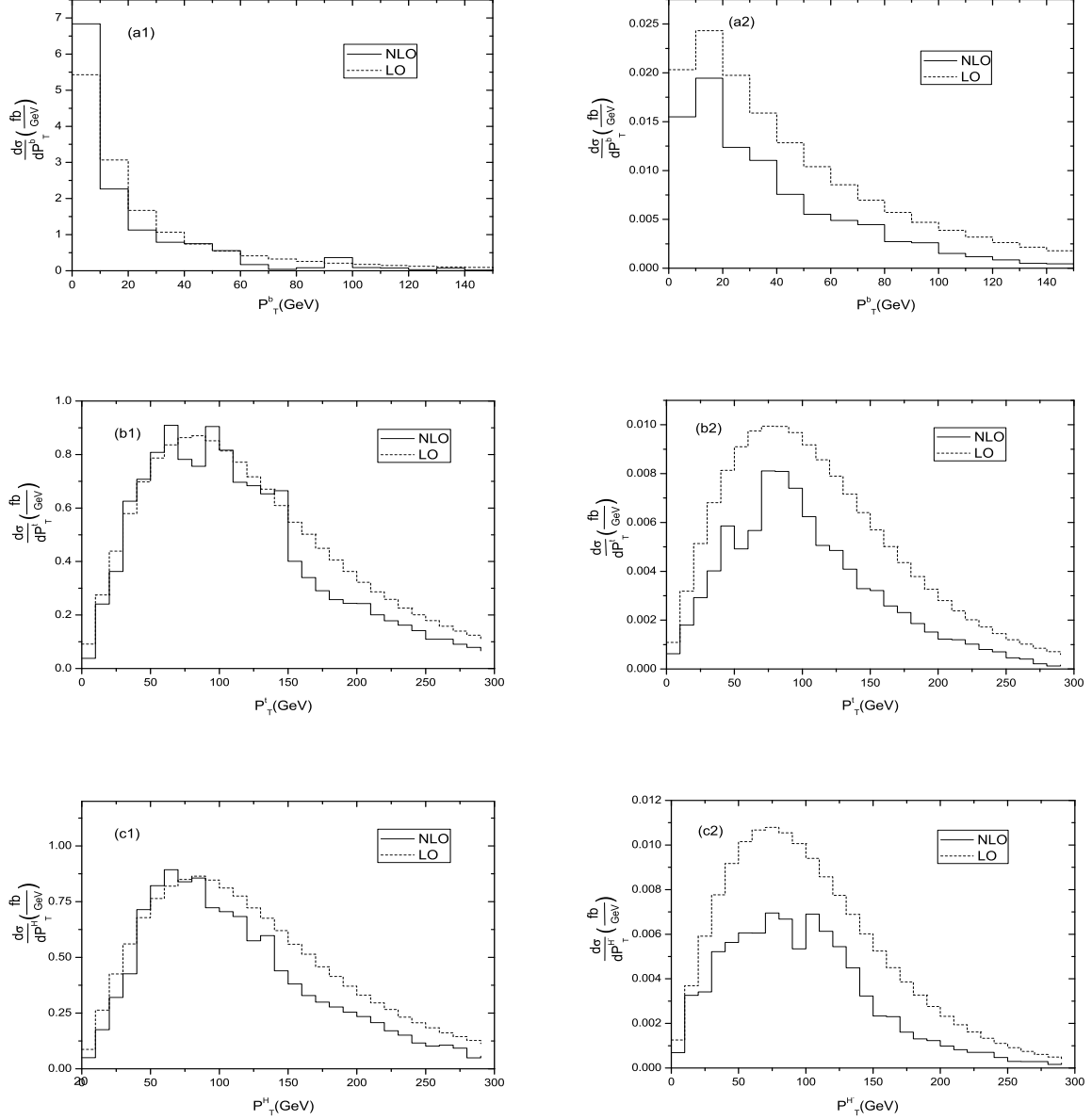


Fig. 9. The transverse momentum distributions of the final state particles(t, \bar{b}, H^-) at LO and NLO of the processes $p\bar{p}/pp \rightarrow t\bar{b}H^- + X$ with $m_{H^-} = 250 \text{ GeV}$ at the LHC and $m_{H^-} = 175 \text{ GeV}$ at the Tevatron. Fig.9(a1, b1, c1) are for the transverse momentum distributions at the LHC and Fig.9(a2, b2, c2) for the transverse momentum distributions at the Tevatron.

References

- [1] S. Weinberg, Phys. Rev. Lett. **19**, 1264 (1967); S. Glashow, Nucl. Phys. **B22**, 579 (1961); A. Salam, in *Elementary Particle Theory*, edited by N. Svartholm, (1968) p367.
- [2] H. P. Nilles Phys. Rep. **110**, 1 (1984); H. E. Haber and G. L. Kane, Phys. Rep. **117**, 75 (1985).
- [3] J. F. Gunion, H. E. Haber, Nucl. Phys. **B272**, 1 (1986).
- [4] F. Abe *et al.* (CDF Collaboration), Phys. Rev. Lett. **79**, 357 (1997); B. Abbott *et al.* (D0 Collaboration), Phys. Rev. Lett. **82**, 4975 (1999).
- [5] Y. Jiang, W.-G. Ma, L. Han, M. Han and Z.-H. Yu, J. Phys. **G24**, 83(1998); Y. Jiang, W.-G. Ma, L. Han, M. Han and Z.-H. Yu, J. Phys. **G23**, 385 (1997), Erratum, *ibidem* **G 23**, 1151 (1997); A. Belyaev, M. Drees, O.J.P. Eboli, J.K. Mizukoshi and S.F. Novaes, Phys. Rev. **D60**, 075008 (1999); A. Belyaev, M. Drees and J.K. Mizukoshi, Eur. Phys. J. C **17**, 337(2000); H.-S. Hou, W.-G. Ma, R.-Y. Zhang, Y. Jiang, L. Han, and L.-R. Xing, Phys. Rev. **D71**, 075014 (2005); S. Moretti, J. Phys. G **28**, 2567(2002).
- [6] E. Eichten, I. Hinchliffe, K.D. Lane and C. Quigg, Rev. Mod. Phys. **56**, 579 (1984) [Addendum-*ibid.* **58**, 1065(1986)]; N.G. Deshpande, X. Tata and D.A. Dicus, Phys. Rev. **D29**, 1527(1984).
- [7] J.F. Gunion, H.E. Haber, F.E. Paige, W.K. Tung and S.S. Willenbrock, Nucl. Phys. **B294**, 621 (1987); S.S.D. Willenbrock, Phys. Rev. **D35**, 173 (1987); A. Krause, T. Plehn, M. Spira and P.M. Zerwas, Nucl. Phys. **B519**, 85 (1998); A.A. Barrientos Bendezu and B.A. Kniehl, Nucl. Phys. **B568**, 305 (2000); O. Brein and W. Hollik, Eur. Phys. J. **C13**, 175 (2000).
- [8] A. Arhrib, M.C. Peyranere, and G. Moultaka, Phys. Lett. **B341**, 313(1995); J. Guasch, W. Hollik, and A. Kraft, hep-ph/9911452.
- [9] Ma Wen-Gan, C.-S. Li, and Han Liang, Phys. Rev. D53, 1304 (1996); S.-H. Zhu, C.-S. Li, and C.-S. Gao, Phys.Rev. D58 (1998) 055007.
- [10] D.A. Dicus, J.L. Hewett, C. Kao and T.G. Rizzo, Phys. Rev. **D40**, 787 (1989); A.A. Barrientos Bendezu and B.A. Kniehl, Phys. Rev. **D59**, 015009 (1998); and Phys. Rev. **D63**, 015009 (2001); O. Brein, W. Hollik and S. Kanemura, Phys. Rev. **D63**, 095001 (2001).
- [11] W. Hollik and S.-H. Zhu, Phys. Rev. **D65**, 075015 (2002).
- [12] J.C. Collins and W.K. Tung, Nucl. Phys. **B278**, 934 (1986); M.A.G. Aivazis, J.C. Collins, F.I. Olness and W.K. Tung, Phys. Rev. **D50**, 3102 (1994); F.I. Olness and W.K. Tung, Nucl. Phys. **B308**, 813 (1988); M. Krämer, F.I. Olness and D.E. Soper, Phys. Rev. **D62**, 096007 (2000).

- [13] K.A. Assamagan, Y. Coadou and A. Deandrea, Eur. Phys. J. **C4**, 1 (2002); P. Salmi, R. Kinnunen, and N. Stepanov, arXiv:hep-ph/0301166; K.A. Assamagan and N. Gollub, arXiv:hep-ph/0406013.
- [14] K.A. Assamagan and Y. Coadou, Acta Phys. Polon. **B33**, 707 (2002); R. Kinnunen and A. Nikitenko, report CMS note 2003/006.
- [15] R.M. Barnett, H.E. Haber and D.E. Soper, Nucl. Phys. **B306**, 697 (1988); A.C. Bawa, C.S. Kim and A.D. Martin, Z. Phys. **C47**, 75 (1990); V.D. Barger, R.J. Phillips and D.P. Roy, Phys. Lett. **B324**, 236 (1994).
- [16] S.H. Zhu, Phys. Rev. **D67**, 075006 (2003).
- [17] E.L. Berger, T. Han, J. Jiang, T. Plehn, Phys. Rev. **D71**, (2005) 115012
- [18] L.Reina, S.Dawson and D.Wackerroth, Phys.Rev. D65 (2002) 053017, arXiv:hep-ph/0109066;
- [19] W.Beenakker, S.Dittmaier, M.Kramer, B.Plumper, M.Spira and P.M.Zerwas, Phys. Rev. Lett. 87 (2001) 201805, arXiv:hep-ph/0107081; Nucl. Phys. B653 (2003)151-203, arXiv:hep-ph/0211352.
- [20] J. Collins, F. Wilczek, A. Zee, Phys. Rev. D 18 (1978) 242; W. J. Marciano, Phys. Rev. D 29 (1984) 580; Phys. Rev. **D31** (1984) 213 (E); P. Nason, S. Dawson, R.K. Ellis, Nucl. Phys. B 327 (1989) 49; Nucl. Phys. B 335 (1989)260 (E).
- [21] M. Carena, D. Garcia, U. Nierste and C.E. Wagner, Nucl. Phys. **B577**, 88 (2000).
- [22] L.J. Hall, R. Rattazzi and U. Sarid, Phys. Rev. **D50** (1994) 7048 [arXiv:hep-ph/9306309]; R. Hempfling, Phys. Rev. **D49** (1994) 6168; M. Carena, M. Olechowski, S. Pokorski and C.E.M. Wagner, Nucl. Phys. **B426** (1994) 269 [arXiv:hep-ph/9402253]; D. Pierce, J. Bagger, K. Matchev and R. Zhang, Nucl. Phys.**B491** (1997) 3,[arXiv:hep-ph/9606211].
- [23] J. Guasch, P. Häfliger and M. Spira, Phys. Rev. **D68**(2003) 115001 [arXiv:hep-ph/0305101].
- [24] P. Häfliger and M. Spira , arXiv:hep-ph/0501164.
- [25] W. Beenakker, R. Höpker, P.M. Zerwas, Phys. Lett. **B378** (1996) 159; W. Beenakker, R. Höpker, T. Plehn, P.M. Zerwas, Z. Phys. **C75** (1997) 349.
- [26] G.Passarino and M.Veltman, Nucl.Phys.B**160**,151(1979).
- [27] J. Kublbeck, M. Bohm and A. Denner, Comput. Phys. Commun. **60**, 165 (1990); T. Hahn, Comput. Phys. Commun. **140**, 418 (2001)140 (2001).
- [28] T. Hahn and M. Perez-Victoria, Comput. Phys. Commun. **118** (1999) 153
- [29] A.Denner and S.Dittmaier, Nucl.Phys.**B658**,175(2003).

- [30] S.Dittmaier, Nucl.Phys.**B675**,447-466(2003).
- [31] G. 't Hooft. M. Veltman, Nucl. Phys.**B153** (1979) 365.
- [32] W. T. Giele and E. W. N. Glover, Phys. Rev. **D46** (1992) 1980 ; W. T. Giele, E. W. Glover and D. A. Kosower, Nucl. Phys. **B403** (1993) 633 ; S. Keller and E. Laenen, Phys. Rev. **D59**, 114004 (1999).
- [33] B.W. Harris and J.F. Owens, Phys. Rev. D **65** 094032(2002).
- [34] G.P. Lepage, J. Comput. Phys. **27**,192(1978).
- [35] H.L. Lai et al. (CTEQ), Eur. Phys. J. **C12**, 375(2000), hep-ph/9903282.
- [36] S. Catani and M.H. Seymour, Phys. Lett. **B378** (1996) 287,[hep-ph/9602277] and Nucl. Phys. **B485** (1997) 291 [Erratum-ibid. B **510** (1997) 291] [hep-ph/9605323].
- [37] S. Catani, S. Dittmaier, M.H. Seymour and Z. Trócsányi, Nucl. Phys. **B627** (2002) 189 [hep-ph/0201036].
- [38] B. C. Allanach *et al.*, in *Proc. of the APS/DPF/DPB Summer Study on the Future of Particle Physics (Snowmass 2001)* ed. N. Graf, Eur. Phys. J. C **25** (2002) 113 [eConf **C010630** (2001) P125] [arXiv:hep-ph/0202233].